CONF-9311140--1

Fast Wave Current Drive Technology Development at ORNL*

by

F. W. Baity, D. B. Batchelor, R. H. Goulding, D. J. Hoffman, E. F. Jaeger and P. M. Ryan

J. S. deGrassie, C. C. Petty, R. I. Pinsker, R. Prater
General Atomics (GA)
P. O. Box 85608
San Diego, CA 92186-9784

Presented at

IAEA Technical Committee Meeting on Radio-Frquency Launchers for Plasma Heating and Current Drive

Naka, Japan
November 10-12, 1993

Prepared for the
Fusion Energy Division
(AT 10 10 14 D)

Prepared by
Oak Ridge National Laboratory
Post Office Box 2008
Oak Ridge, TN 37831-6285 USA

Managed by
MARTIN MARIETTA ENERGY SYSTEMS, INC.

for the
U.S. DEPARTMENT OF ENERGY
under contract DE-AC05-84OR21400

* Research sponsored by the Office of Fusion Energy, U.S. Department of Energy, under contract DE-AC05-84OR21400 with Martin Marietta Energy Systems, Inc.

FAST WAVE CURRENT DRIVE TECHNOLOGY DEVELOPMENT AT ORNL*

F. W. BAITY, D. B. BATCHELOR, R. H. GOULDING, D. J. HOFFMAN,
E. F. JAEGER, P. M. RYAN
Oak Ridge National Laboratory, Oak Ridge, Tennessee, USA

J. S. DEGRASSIE, C. C. PETTY, R. I. PINSKER, R. PRATER
General Atomics, San Diego, California, USA

ABSTRACT

The technology required for fast wave current drive (FWCD) systems is discussed. Experiments are underway on DIII-D, JET, and elsewhere. Antennas for FWCD draw heavily upon the experience gained in the design of ICRF heating systems with the additional requirement of launching a directional wave spectrum. Through collaborations with DIII-D, JET, and Tore Supra rapid progress is being made in the demonstration of the physics and technology of FWCD needed for TPX and ITER.

INTRODUCTION

Steady-state current driven by fast waves in the ion cyclotron range of frequencies (ICRF) is predicted to have comparable efficiency to other possible current drive methods for break-even plasmas. The requirement of driving current places the additional demand of asymmetric phasing on ICRF systems. Maximizing the current drive involves a tradeoff between maximizing the current drive efficiency of the antenna and maximizing the power handling. Reduction of impurities with asymmetric phasing is also a concern.

Given the interaction between the antenna and the plasma edge, it is important to have realistic models of the fields produced by the antenna, including 3-D effects, and of the wave behavior in the plasma including details of the edge region. A number of tools have been developed to optimize the design and performance of FWCD antennas. These include modeling the effects of slots in the antenna sidewalls, modeling the current drive efficiency in plasma with realistic antenna geometry, and modeling the coupled transmission line systems with decouplers. In addition, bench testing of FWCD antennas has been conducted to verify the models and to develop practical tuning and matching algorithms.

Experiments have been underway since 1990 with a single four-element FWCD array on DIII-D operating at 60 MHz. During this time a number of modifications have been made both to the antenna and to the external matching circuit in order to optimize performance. In collaboration with JET, modeling and design of power compensators for the JET A_2 antennas has been undertaken. Some form of power compensation is required in order to operate at full source power whenever the phasing between elements is other than 0° or 180°. A prototype system has been tested on DIII-D. Two new 4-element FWCD antennas under construction for DIII-D are designed to have pulse lengths of 10 s

* Research sponsored by the Office of Fusion Energy, U.S. Department of Energy, under contract DE-AC05-84OR21400 with Martin Marietta Energy Systems, Inc.

and to operate at up twice the power of the existing FWCD antenna in the frequency range of 30 to 120 MHz.

PROOF-OF-PRINCIPLE ANTENNA FOR DIII-D

The first embodiment [1,2] of the present four-strap antenna array on DIII-D, shown in fig. 1, was designed in 1989. The array occupies a 1.0-m × 0.5-m recess in the vacuum vessel wall with coaxial feeders extending out through two separate ports. The array consists of two enclosures, each housing two straps, mounted side by side. Each enclosure was covered by a two-tier Faraday shield of copper-plated Inconel 625 rods coated with 10 μm of Ti(C,N). Between each pair of straps was a slotted septum giving coupling coefficients of 4% (between straps 2 and 3) and 7% (between straps 1 and 2 and between straps 3 and 4). These values of mutual coupling were chosen based on the anticipated plasma loading and to be able to maintain arbitrary phasing between adjacent straps.

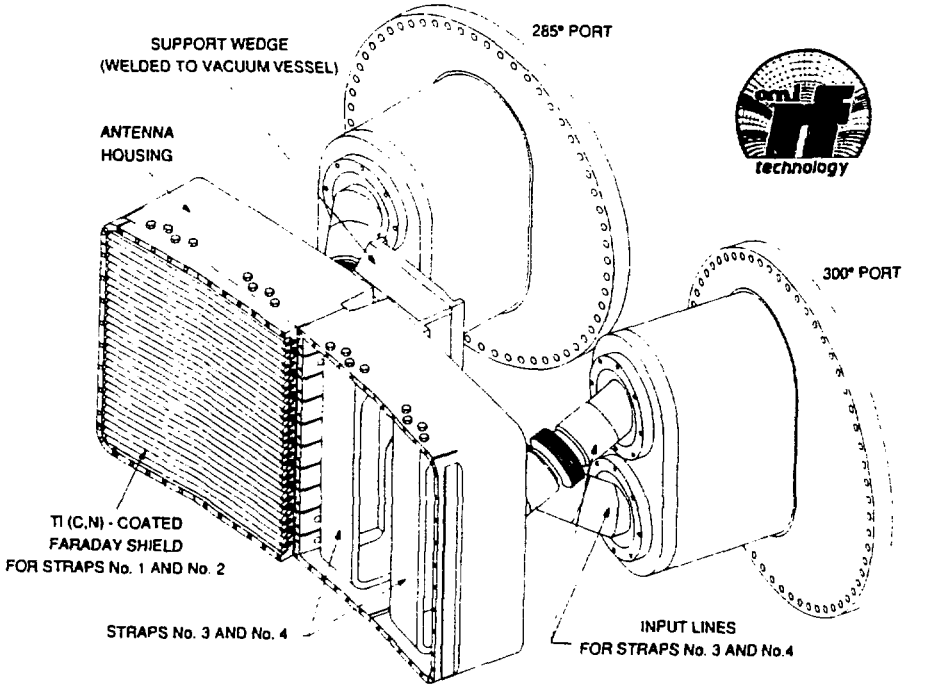

Fig. 1. Fast wave current drive antenna for DIII-D (30-60 MHz, 2 MW, 2 s, four strap)

The antenna is powered from a single RF transmitter having a nominal output of 2 MW from 30 to 60 MHz. A full-scale mockup of the array was used for measurements of antenna parameters and for developing phasing and impedance matching algorithms. Two phasing circuits were proposed: one, employing eleven tuning elements, provided the capability of arbitrary phasing between adjacent straps, and the other, employing five tuning elements, provided the capability of phasing at only 0°, ±90° or 180° between straps [3,4]. The latter circuit was implemented on DIII-D, both to save cost and to reduce the complexity of phasing and matching as much as possible for initial experiments. Figure 2 is a schematic drawing of the circuit used on DIII-D.

Experiments from plasma operation on DIII-D [5-7] led to the conclusion that antenna performance could be improved by increasing the mutual coupling between adjacent straps. Accordingly, the antenna was modified by removing the slotted septum separating the two straps in each enclosure and by deepening the slots between the two enclosures. This increased the coupling coefficients to 7% and 9%.

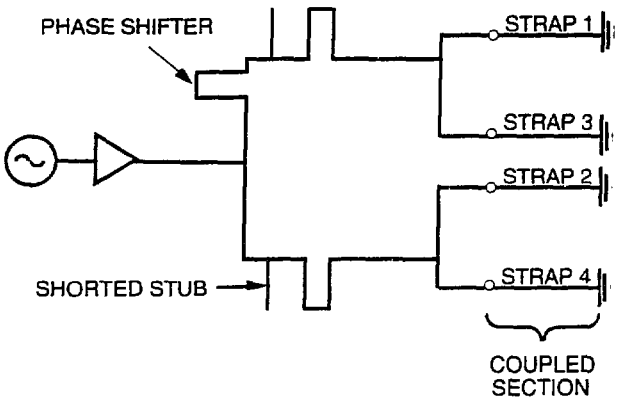

Fig. 2. The phasing and impedance matching circuit used in the initial FWCD experiments on DIII-D.

In addition it was found that the impurity generation from the Faraday shield at 90° phasing, as evidenced by Ti radiation, was almost the same as 0°, whereas impurity generation is minimized at 180° phasing. In order to reduce impurity production as much as possible, it was decided to take advantage of two new developments: boronization of the vacuum vessel and coating the Faraday shield with B_4C. The early boronization system on DIII-D consisted of two diborane feeds, one through the antenna port and the other on the opposite side of the tokamak. Meanwhile, plasma spraying of B_4C had been under development at Cadarache, France and was used on new Faraday shields installed on Tore Supra. High heat flux testing of this B_4C coating was conducted at ORNL with excellent results, exceeding the capabilities of Ti(C,N).

Therefore, a new Faraday shield was installed, having a single-tier of copper-plated Inconel rods angled at 12° to the horizontal in order to align the elements with the static magnetic field at the antenna location under normal plasma operating conditions. The new shield, following recent ICRF practice, has an optical transparency of 45%, and was coated with 100 μm of B_4C at SNMI (Avignon, France). Figure 3 is a photograph of the new Faraday shield. The combination of the new Faraday shield coating and boronization of the entire vacuum vessel has reduced impurities to negligible levels.

With the new configuration the antenna has been operated at 1.6 MW and up to 90% of the design joule limit. The power limit appears related to interactions between the edge plasma and the B_4C coating, often with the release of macroscopic flakes into the plasma. The flaking is primarily restricted to one of the two Faraday shields. This shield has a B_4C coating which is thicker than the specified 100 μm, and the additional thickness may be responsible for the poorer bonding.

Between the time of the removal of the original Faraday shield and the installation of the single-tier shield, the antenna was operated in plasma without a Faraday shield for a brief period. Experimental time during the shieldless operation was insufficient to draw firm conclusions, but two observations of note were that: (1) the power limit of the antenna was lower than it was with a Faraday shield, although the limiting mechanism was not identified, and (2) impurities (primarily copper) did not increase.

ANTENNA ANALYSIS

A number of codes have been written or adapted to aid in the design of FWCD antennas [8]. The goal is to determine the basic parameters of the antenna in the presence of plasma, such as the self and mutual inductance, capacitance, and loading per unit length of the current strap. These parameters are used as inputs for transmission line analysis of the remainder of the system. This provides the ability to determine the net power delivered to the plasma and the electrical load that the antenna will present to the power distribution system, in order to predict currents, voltages, and heat loads throughout the system.

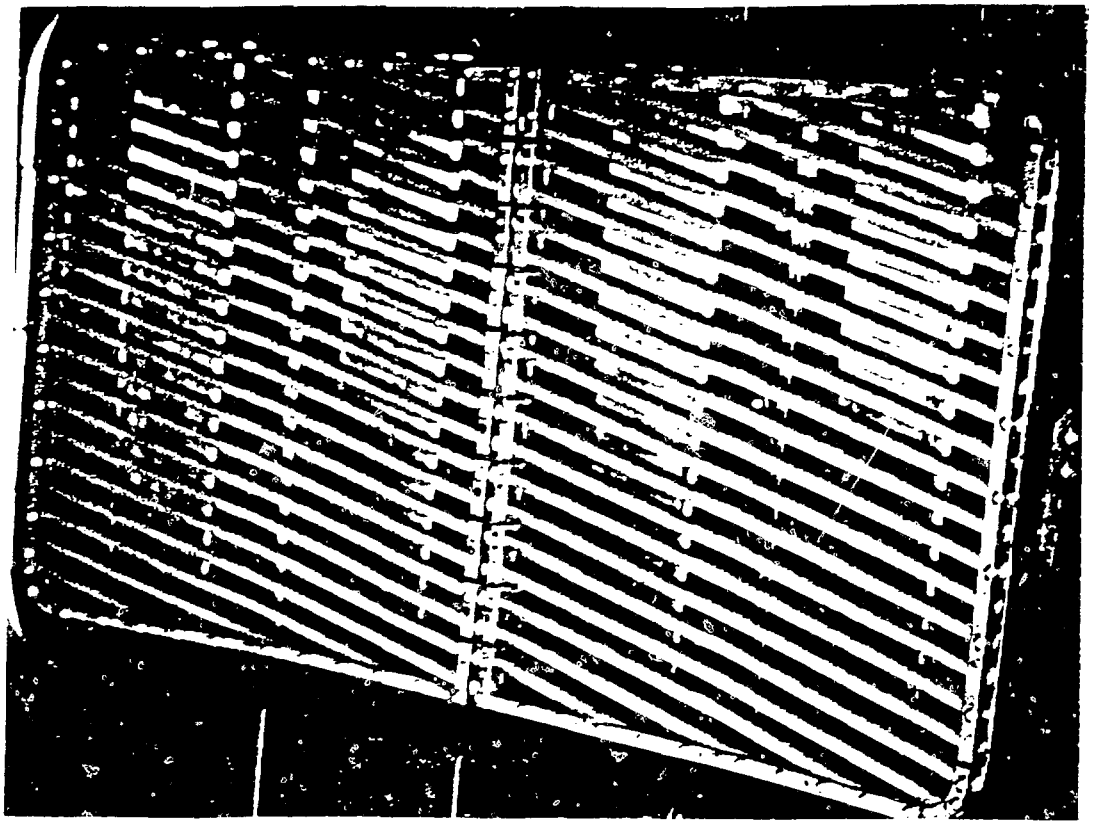

Fig. 3. New B_4C-coated Faraday shield for DIII-D. The shield is tilted at 12° to align with the magnetic field lines at the antenna location. Visible at the right side are the horns of a microwave reflectometer for measurements of the edge density.

The effects of the enclosure surrounding the current strap, the finite poloidal extent of the strap, and the influence of the Faraday shield have been modeled with two-dimensional and three-dimensional magnetostatic codes. The influence of the ends of the antenna enclosure and the current strap configuration are shown in fig. 4 for the case of the long-pulse FWCD antennas for DIII-D. This calculation assumes constant current in the poloidal direction (low-frequency limit) so that the shape of the curves is due solely to geometric effects. The factor α is the length attenuation due to a given geometry. Finite wavelength effects cause additional reduction in the effective length of the current strap. The Faraday shield effect on phase velocity must be known in order to calculate this factor. Figure 5 shows the effects of finite wavelength at 120 MHz for the same geometry as in fig. 4.

Heating of the Faraday shield from a combination of plasma bombardment and RF dissipation is often the limiting factor in antenna operation. The heating from RF-induced currents can be of concern for FWCD antennas due to the advantages for directionality of operating with larger antenna-to-plasma gaps.

Modeling the influence of sidewall currents is crucial in determining the directionality of the wave spectrum generated by a FWCD array. Return currents in the antenna sidewalls generate waves with high $k_\parallel$ traveling in the opposite direction to the main peak launched by the antenna, as shown in fig. 6. While the undesired peak at high reverse $k_\parallel$ evanesces more rapidly than the low $k_\parallel$ peak, these currents lead to higher voltages in the antenna structure and therefore to lower power limits.

Finally, the wave spectrum determined by the three-dimensional antenna modeling becomes the source term for PICES [9], a three-dimensional full-wave plasma code, to calculate power deposition profiles and current drive efficiency.

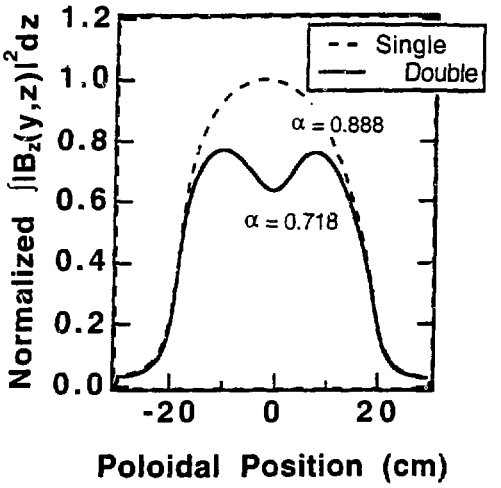

Fig. 4. The effect on the toroidal magnetic flux 2.5 cm in front of the current strap of finite poloidal extent of the strap for single and double strap configurations with the dimensions of the long-pulse FWCD for DIII-D. This calculation was made in the low frequency limit (uniform current in the strap). α is the attenuation factor resulting from purely geometrical effects.

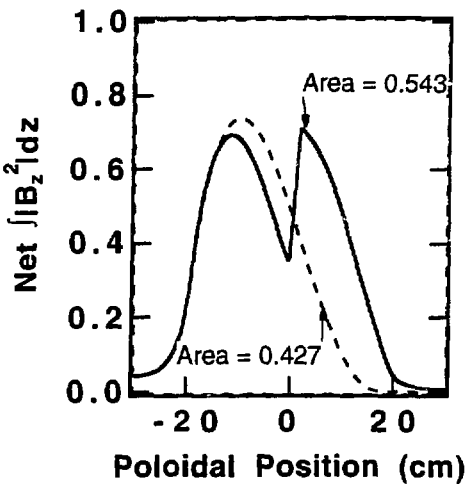

Fig. 5. The combined effects of finite wavelength at 120 MHz and finite poloidal extent on the toroidal magnetic flux 2.5 cm in front of the current strap for the same geometry as in fig. 4. The double strap configuration produces 25% more loading than the single strap configuration at this frequency.

Fig. 6. Electric fields in the plasma generated by a four-strap array phased at 90° for DIII-D conditions as calculated by the two-dimensional cold plasma recessed antenna code, RANT. Low-$k_{||}$ waves in the forward direction result from the currents on the straps. The smaller-amplitude, high-$k_{||}$ waves in the reverse direction result from the return currents in the sidewalls.

DECOUPLER DESIGN

The phasing and matching circuit used for the first experiments on DIII-D is shown in Fig. 2. The resonant loops combining straps 1 and 3 and straps 2 and 4 reduce the system to a two-port network. The power in the two feed lines is unbalanced when operated with equal strap currents at a phase other than 0° or 180° due to the mutual coupling between straps. This uneven power split necessitates the use of an unmatched tee at the transmitter end. The ratio of the powers in the two lines for equal antenna currents at 90° is given by

$$\frac{P_A}{P_B} = \frac{1 - kQ}{1 + kQ},$$

where k (≡M/L) is the effective coupling coefficient between the two lines and Q is the quality factor. The condition kQ = 1, where all the power appears in line B, corresponds to a series resonant load resistance of approximately 1.5 Ω for the present DIII-D configuration. The term series resonant load resistance refers to the value of the impedance measured one-quarter wavelength ahead of the resonant loop tees. For kQ > 1 the circuit is unstable and difficult to control. The loading resistance under typical FWCD operating conditions on DIII-D is of this order, so the powers are typically substantially unbalanced.

A decoupler which effectively cancels the effects of the mutual coupling between straps can be added to provide an equal power split between the two feed lines. A decoupler is advantageous whether in a system like DIII-D, where an antenna array is fed from a single RF source or like JET, where separate sources are used for each array element. In the case of separate power sources per element a decoupler is required in order to operate at full power. ORNL and JET are collaborating on modeling and design of a decoupler arrangement for use with the JET A_2 antenna arrays [10-13].

A prototype decoupler has been tested on the DIII-D system [11,14]. The decoupler, consisting of an 80-mm-diameter, 50-Ω, 3-dB hybrid junction with two ports terminated with tunable stubs, was connected at the resonant loop tees, which are at a voltage maximum, as shown in fig. 7. When the decoupler is exactly tuned, the power transferred from one resonant loop to the other circulates through the decoupler, resulting in an equal powers in the two feed lines for all phase angles. This was demonstrated during plasma operation, as shown in fig. 8, when the phase between the resonant loop tees was varied through 360° without readjustment of any tuning elements on a sequence of fourteen plasma shots where the antenna loading resistance was maintained at 1.5 Ω. The RF power was 0.1 MW on all shots.

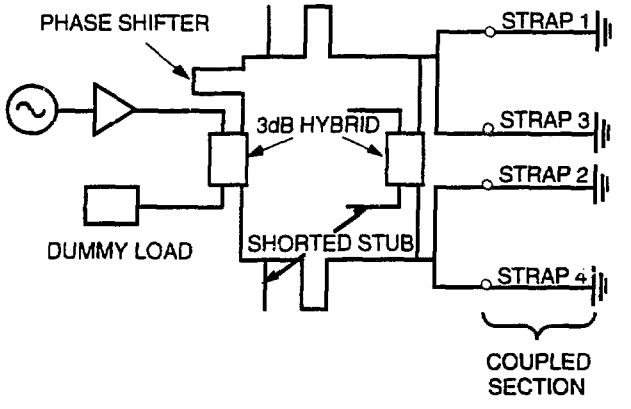

Fig. 7. The phasing and impedance matching circuit used for the prototype decoupler tests on DIII-D.

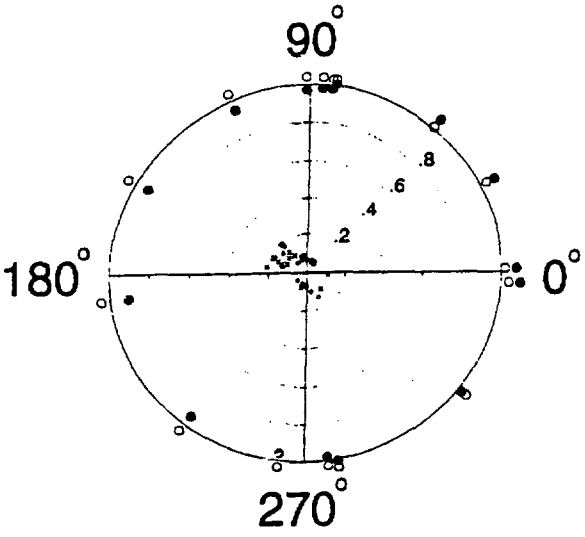

Fig. 8. 14-shot phase scan with the decoupler tuned. The solid circles are the ratio of the voltages at the two resonant loop tees, the open circles are measured on the generator side of the matching network. The ×'s and ◊'s are the reflection coefficients on the generator side of the two feed lines. No adjustments of the matching network were made during the scan.

LONG-PULSE FWCD ANTENNAS FOR DIII-D

Two long-pulse FWCD antennas for DIII-D have been designed [15] and will be installed in early 1994. These antennas will increase the available FWCD power from 2 MW to 6 MW for pulse lengths of up to 2 s, and to 4 MW for up to 10 s. When operated at 90° phasing into a low-density plasma ($\sim 4 \times 10^{19}$ m^{-3}) with hot electrons (~10 keV), the two new antennas are predicted to drive approximately 1 MA of plasma current. Specifications for these antennas are given in Table 1.

The antennas incorporate extensive water cooling. The Faraday shield, however, is uncooled, and is the primary factor limiting the pulse length. The new antennas are designed to mount at the 0° and 180° toroidal locations in ports originally housing movable limiters. These ports restrict the width of the arrays to 75 cm. All four coax feeds pass through a single port. The antennas are modular, with separate water feeds for each array element, simplifying installation and maintenance. All internal surfaces are nickel plated.

Table 1. DIII-D Long-Pulse FWCD Antenna Specifications

Maximum power	2 MW (4 MW with second RF source)
Maximum pulse length	10 s
Number of array elements	4
Frequency range	30-120 MHz
Phasing (between adjacent elements)	0°, ±90°, 180°
Dimensions	75 cm × 46 cm

The Faraday shield consists of a single layer of 13-mm-diameter nickel-plated molybdenum rods with a 100-μm-thick plasma sprayed coating of boron carbide on the plasma-facing side. The rods are inclined at a 12° angle to match the pitch of the local magnetic field at the shield location. The rods are mounted to the antenna housing individually by thin Inconel strips to allow for differential thermal expansion of the Faraday shield relative to the antenna housing. The length of the Inconel strips was chosen to provide the desired magnetic coupling between adjacent antenna elements.

Figure 9 is a front view of the antenna array, showing the four elements with the feed lines extending to the vacuum feedthroughs at the port cover flange.

At the upper frequency of operation of 120 MHz, the electrical length of a single current strap with a phase velocity of 0.6c (due to the Faraday shield) is longer than a

quarter wavelength. Since there is not room for two coaxial feeds per element, the current strap is divided into two poloidal segments. Three-dimensional modeling of the RF magnetic field amplitudes was used to compare the double strap configuration to a single strap at 60 and 120 MHz. The poloidal distributions of the integrated toroidal magnetic flux are shown in Fig. 10. The double strap produces more total flux at the plasma boundary at 120 MHz, whereas the single strap is superior at 60 MHz. However, the double strap configuration results in a lower voltage between the antenna and Faraday shield than a single strap, so the double strap is practically equivalent to the single strap even at 60 MHz. Below 60 MHz the double strap exacts a penalty, but the antenna design was optimized for higher frequency operation.

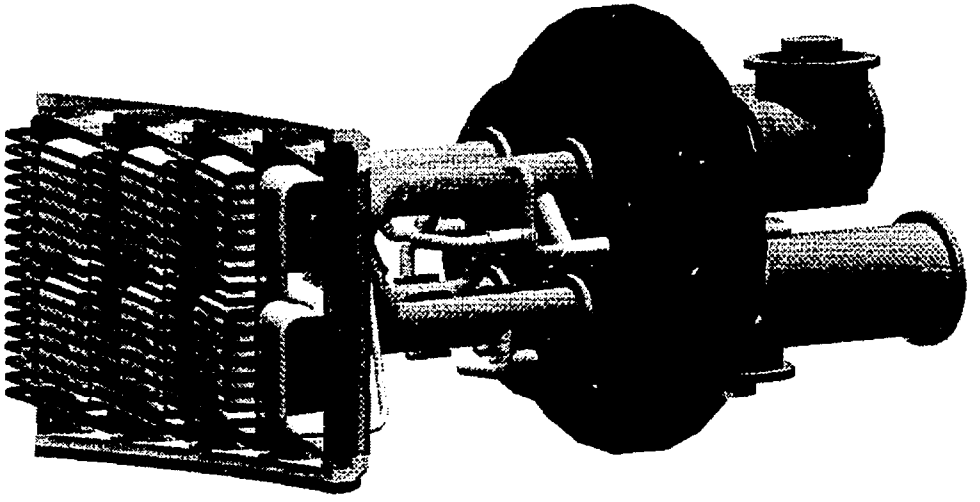

Fig. 9. Long-pulse FWCD antenna for DIII-D.

The maximum power capability of the antenna with a peak voltage of 30 kV appearing anywhere in the antenna structure is shown in Fig. 11 as a function of antenna loading resistance for 60, 90, and 120 MHz. The value plotted is the total power for the array with the 30–kV peak voltage occurring on any element of the array at 90° phasing.

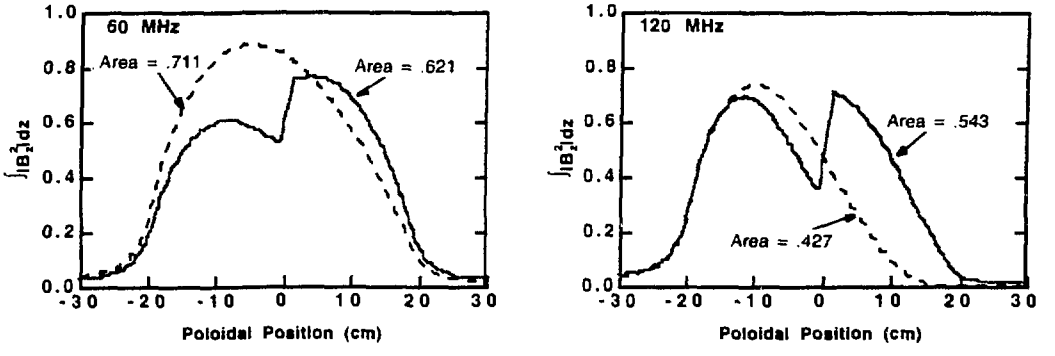

Fig. 10. Net $\int |B_z|^2 dz$ distribution 2.5 cm in front of the current strap for single and double strap configurations at 60 and 120 MHz.

The wide frequency range of operation causes voltage and current maxima to occur throughout the transmission line. In particular, the vacuum feedthrough is near a voltage minimum at 120 MHz, but near a voltage maximum at 60 MHz. Thus, all components must be designed to handle high voltages. Based on superior voltage standoff in feedthrough tests conducted at ORNL [16] comparing copper, nickel, silver, and gold electrodes, nickel plating was selected for all components in vacuum.

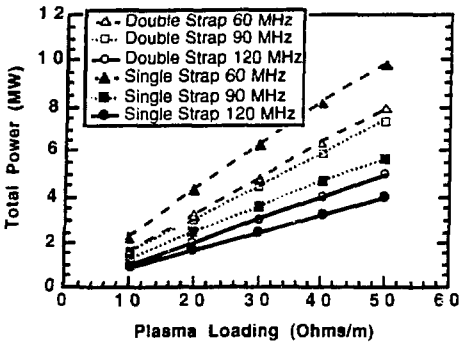

Fig. 11. Maximum power per array as a function of plasma loading with a 30 kV peak voltage limit for 60, 90, and 120 MHz.

The external transmission line system will be of the same basic design as that used successfully on the existing FWCD antenna on DIII-D with some refinements [17]. The circuit is shown schematically in Fig. 12. The loops connecting modules 1 and 3 and modules 2 and 4 are adjusted to produce phasing of either 0° or 180° between alternate modules. The decoupler stub balances the power on the two feed lines and the susceptance null stubs result in a purely real impedance at the output of the quarter-wave transformers.

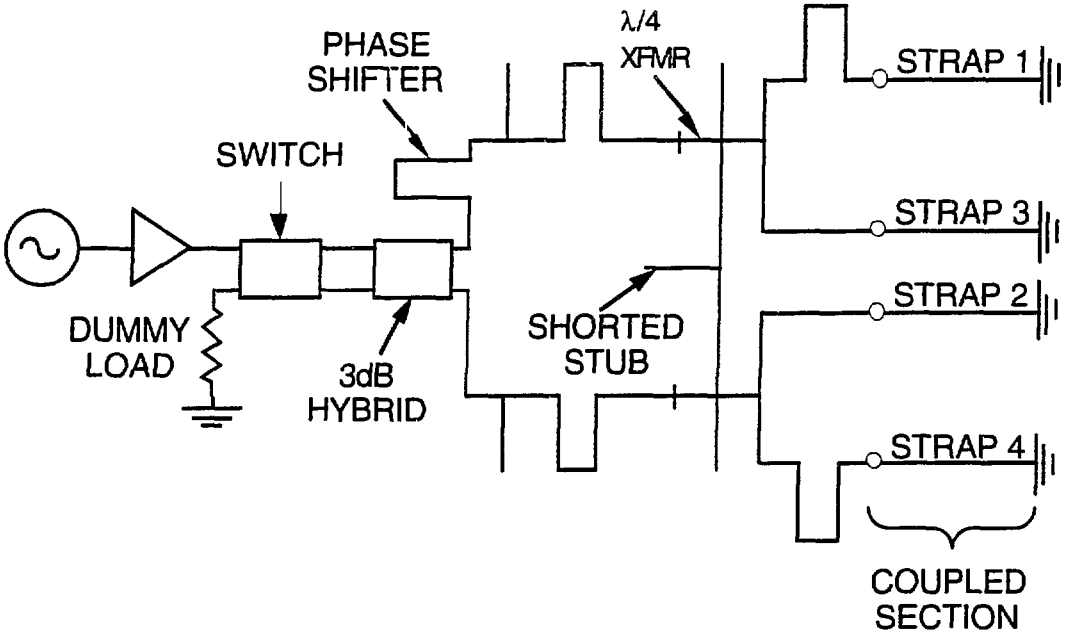

Fig. 12. The tuning and matching circuit, incorporating a single-stub decoupler and quarter-wave transformers, to be used with the long-pulse FWCD antennas.

SUMMARY

The technology of FWCD systems is being advanced rapidly through the development of new tools to analyze complex antenna structures in three dimensions and through the design and manufacture of antenna arrays and phase control systems. The interaction of the plasma with the antenna requires accurate modeling of the entire FWCD system and of the plasma response. Experiments on DIII-D and elsewhere have demonstrated key aspects of FWCD, although at fairly modest levels to date. With new high-power FWCD antennas due to become operational on both DIII-D and JET in 1994, the experimental validation of FWCD needed for implementation on future tokamaks can be expected in the near future.

ACKNOWLEDGEMENTS

The authors gratefully acknowledge the assistance of B. Beaumont, J.-P. Cocat, E. Gauthier, and R. Gravier of CEN-Cadarache for arranging the B_4C coating of the Faraday shield for the DIII-D antennas. We also wish to acknowledge the contribution of our colleagues at JET: V. Bhatnagar, G. Bosia, M. Bures, J. A. Dobbing, D. F. H. Start, and T. J. Wade.

REFERENCES

[1] F. W. Baity et al., in Fusion Technology 1990, (North Holland, Amsterdam, 1990), vol. 2, p. 1035.

[2] R. H. Goulding et al., in Proc. 17th Europ. Conf. on Controlled Fusion and Plasma Physics, Amsterdam, 1990 (European Physical Society, Petit-Lancy, 1990) vol. 14B, part III, p. 1311.

[3] R. H. Goulding et al., "Phased operation of the DIII-D FWCD antenna array with a single power source," to be published in Fusion Engineering and Design.

[4] R. I. Pinsker et al., in Proc. 14th IEEE/NPSS Symp. on Fusion Engineering, San Diego, 1991 (IEEE 91CH3035-3, Piscataway, NJ, 1992) vol. I, p. 115.

[5] C. C. Petty et al., Phys. Rev. Let. 69 (1992) p. 289.

[6] R. I. Pinsker et al., in Plasma Phys. and Contr. Fusion Research 1992, (IAEA, Vienna, 1993) Vol. I, p. 683.

[7] R. Prater et al., in Proc. IAEA Tech. Comm. Meeting on Fast Wave Current Drive in Reactor Scale Tokamaks, Arles, 1991 (Association EURATOM-CEA, Centre d'Etudes Nucléaires de Cadarache, 1991) p. 308.

[8] P. M. Ryan et al., "Methods of calculating selected geometrical effects in the design of ICRH antennas," to be published in Fusion Engineering and Design.

[9] E. F. Jaeger et al., Nucl. Fusion 33 (1993) p. 179.

[10] R. H. Goulding et al., in Fusion Technology 1992, (North Holland, Amsterdam, 1993) p. 515.

[11] R. H. Goulding et al., "Power compensators for phased operation of antenna arrays on JET and DIII-D," in Radiofrequency Power in Plasmas: Proc. 10th Topical Conf., Boston, 1993, to appear.

[12] R. H. Goulding et al., "Design and control of phased ICRF antenna systems," in Proc. 15th IEEE/NPSS Symp. on Fusion Engineering, Cape Cod, October 11-15, 1993, to appear.

[13] A. G. H. Sibley et al., "Power optimisation in the rf systems in JET and future systems," in Proc. 15th IEEE/NPSS Symp. on Fusion Engineering, Cape Cod, October 11-15, 1993, to appear.

[14] R. I. Pinsker et al., "Experimental test of a two-port decoupler in the DIII-D fast wave current drive system," in Proc. 15th IEEE/NPSS Symp. on Fusion Engineering, Cape Cod, October 11-15, 1993, to appear.

[15] F. W. Baity et al., "Design of long-pulse fast wave current drive antennas for DIII-D," in Radiofrequency Power in Plasmas: Proc. 10th Topical Conf., Boston, 1993, to appear.

[16] F. W. Baity et al., in Proc. 13th European Physical Society Conference on Controlled Fusion and Plasma Heating, Schliersee, 1986 (European Physical Society, 1986) vol. 10C, part II, p. 157.

[17] J. S. deGrassie et al., "4 MW upgrade to the DIII-D fast wave current drive system," in Proc. 15th IEEE/NPSS Symp. on Fusion Engineering, Cape Cod, October 11-15, 1993, to appear.